# DEVELOPMENT OF ULTRASONIC MODELS FOR HARD-ALPHA INCLUSIONS IN TITANIUM ALLOYS

Chien-Ping Chiou, Frank J. Margetan, R. Bruce Thompson,
and Brian Boyd
Center for Nondestructive Evaluation and
Iowa State University
Ames, Iowa 50011

## INTRODUCTION

This paper describes research directed towards modeling ultrasonic signals from hard-alpha inclusions in titanium alloys. The modeling effort has been made difficult by the complicated morphology of such inclusions which can include voids, cracks, core and diffusion zones. Fortunately, a large portion of hard-alpha inclusions are acoustically weak scatterers in nature, and advantage can be taken of simplifications as afforded by Born approximation and some ad-hoc interface conditions. Models along these lines have been previously developed and their validations on synthetic hard-alpha inclusions of cylindrical shape at normal incidence have been reported [1]. Extensive use of these ultrasonic models were also presented in the development of a statistical methodology for estimating the probability of detection [2,3]. In current work, we extend the model capability to include arbitrary flaw orientation and oblique incidence. Model predictions are compared with experimental data collected from titanium specimens for different beam angles, focal depths, inclusion sizes and orientations. The range of the model applicabilities and their possible extensions will be presented. Morphological modeling of the three-dimensional, naturally-occurring inclusions based on stacks of two-dimensional metallographic measurements are also described.

## MODELING THEORY

The ultrasonic modeling considered here follows a similar approach to the Thompson-Gray measurement model [4]. By utilizing Auld's reciprocity relationship [5], this approach is capable of relating the field measurements to a series of frequency domain sub-modules, each modeling one aspect of the ultrasonic phenomena occuring in an inspection process. The product of these sub-modules is evaluated within the transducer bandwidth, and then converted back to time domain through numerical Fourier synthesis. The time domain signals can be directly compared with the rf waveform measurements as obtained from an oscilloscope. The main advantage of taking this approach is the reduction of computation effort while maintaining necessary modeling complexity. The use of Gauss-Hermite beam model [6], for example, enables the wave fields be rapidly calculated in the regions of interest. In contrast with other numerical methods such as finite element and boundary element, this beam model consumes much less computation time by many orders-of-magnitude.

*Review of Progress in Quantitative Nondestructive Evaluation, Vol. 16*
Edited by D.O. Thompson and D.E. Chimenti, Plenum Press, New York, 1997

Two new models developed for cylindrical inclusions have been previously reported [1]. The first is an ad-hoc surface model which applies Kirchhoff approximation-like boundary conditions on the inclusion-host interfaces and carries out the computation by two-dimensional numerical integration at the interfaces. The formulation is similar to that of our previous flat-bottom hole study [7] with an additional integration for the inclusion back wall and a factor accounting for the time delay between the front and back walls. The second model is a volumetric formulation utilizing the Born approximation and a three-dimensional numerical integration scheme. This model has the most technological importance because of its applicability to weak inclusions of arbitrary compositions and geometries if information regarding elastic moduli and density are available everywhere within the volumetric boundaries. In the past period, we have further extended the model's capacity to include arbitrary orientation at oblique incidence. This was done using sequential coordinates transformations from the original fixed geometry. The ad-hoc surface model, while giving a faster method in obtaining waveform calculations, however, is limited to normal incidence due to a modeling deficiency at high incident angles. In this regard, Born model certainly provides much wider range of applicability, but requires computation time one order-of-magnitude higher.

For an inhomogeneous inclusion embedded in an otherwise isotropic, homogeneous material, the relationship between frequency domain displacement of the Born model signal $u(\omega)$, the incident wave field $u^{inc}(\underline{y},\omega)$ and a material function $f(\rho,c)$ can be expressed by:

$$u(\omega) \propto \iiint_V [u^{inc}(\underline{y},\omega)]^2 f[\rho(\underline{y}),c(\underline{y})]d\underline{y} \tag{1}$$

in which superscript "inc" represents the incident field, $\omega$ is the radial frequency, and $\rho$ and $c$ are the density and longitudinal wave speed within the inclusion volume v, respectively. In the ordinary context of the Born approximation, both the density and wave speed are assumed to be very close to those of the host materials, i.e. the flaw is assumed to possess a weak (small) impedance mismatch. Intuitively, this weak impedance assumption is consistent with the Born approximation that replaces the wave field quantities within the inclusion by the incident field counterparts. However, from a comparative study with the high-frequency Kirchhoff approximation, both approximations have been shown to be equivalent in modeling the leading specular (front surface) responses. As such, it has become unnecessary to impose this weak impedance assumption. The material function in Eq. (1) with and without the weak impedance assumption are referred below as "weak Born model" and "normal Born model":

$$f(\rho,c) = 2\rho_h\left(\frac{c_f - c_h}{c_h} + \frac{\rho_f - \rho_h}{\rho_h}\right) \quad \text{for weak Born model} \tag{2}$$

$$f(\rho,c) = \rho_f\left(\frac{c_f^2 + c_h^2}{c_h^2}\right) - 2\rho_h \quad \text{for normal Born model} \tag{3}$$

where subscript h represents the titanium host media, and f denotes the hard-alpha inclusion. The difference between Eqs. (2) and (3) in comparison with the experiment will be discussed in next section.

## SYNTHETIC HARD-ALPHA EXPERIMENT

The validation of the ultrasonic models described above were continued using experimental data obtained from the same seeded titanium sample used before [1]. In particular, a rectangular block of 10.125"Lx4.75"Wx3"H, fabricated from Ti-6Al-4V ring forging was tested in the experiment. A total of 32 synthetic hard-alpha (SHA) inclusions ranging from #2 (2"/64) to #5 (5"/64) with 8 of each size were inserted into the test block at 1" depth, normal to the front surface by hipping procedures. These SHA's were specially manufactured in cylindrical shape (with the diameter same as the height) from pure titanium of 5.88 wt.% nitrogen and 0.465 wt.% oxygen content. Two focused broadband immersion transducers were used for comparison. The first (hereafter referred as transducer A) has a central frequency at 5 MHz, 1" in diameter and a focal length of 8.4" in water. The second (transducer B) is a 10 MHz 1.5" diameter probe with a focal length of 9.3". A 3x3 waterpath-transducer tilt angle combinations were selected from the experimental design in order to attain sufficient variations of these inspection parameters. Additional data were taken from the row of 8 #5 SHA's on one LxH side of block. In this configuration, the SHA's were scanned at their circumferential (side-on) surfaces.

Fig. 1 plots the peak-peak amplitudes of averaged experimental data and model predictions vs. various SHA sizes. In this case, transducer A was operated at normal incidence, focused on SHA's at 1" depth. Good agreement is clearly observed between the model and experiment. The only exception is for size #2 at which, as was previously reported [1], the model predictions are actually compared with experimental data on the noise floor. The improvement in amplitude accuracy of normal Born model (Eq. (3))over the weak Born model (Eq. (2)) is also significant. The waviness at the lower ends of model curves is likely due to the phase cancellation/amplification between the inclusion front and back wall echoes whose timing happens to coincide with the specific inclusion sizes in that region. This event has been noted in our earlier flat-bottomed hole analysis [7].

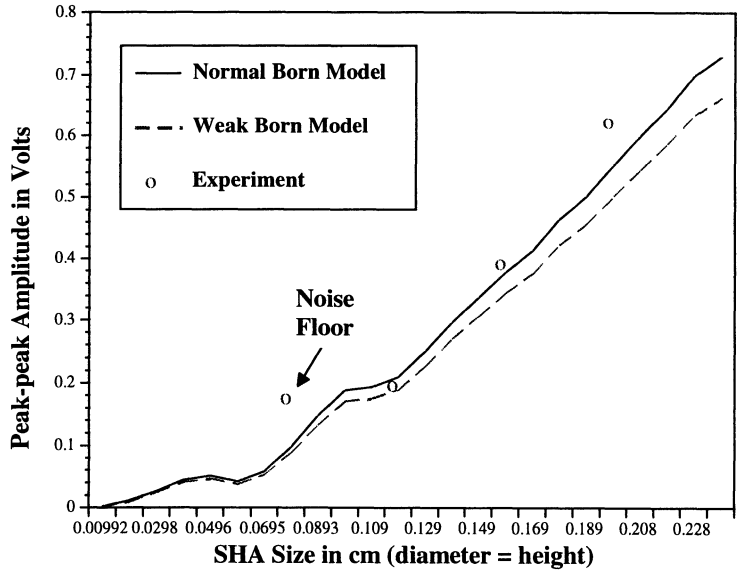


Figure 1. Peak-peak signal comparisons between two models and experiment using transducer A at normal incidence, focused on SHA's at 1" depth.

The summary of model predictions and corresponding experiment results are given in Table 1 for all cases at three focal depths and three tilt angles using transducer A. Model predictions show overall good agreement with experimental data though underestimate in most cases. Since the higher impedance mismatch between the SHA and host titanium is beyond the Born model limit, this underestimate situation is as expected and has been confirmed by a separate comparison between the Born model and an exact solution pertaining to spherical inclusion [1]. Also note that the comparisons between model and experiment are no longer valid for cases having either missed data or noise floor (see indications by M or N in Table 1).

Fig. 2 compares the rf waveforms of an experimental measurement with normal Born model predictions for a typical #5 SHA focused at normal incidence using transducer B. Good agreement is also seen in both the absolute amplitude and phase between model and the experiment. The slight time delay of the phase-reversed back wall echo comes from the direct application of the incident wave throughout the inclusion body, which does not include the wave speed difference between the inclusion and the host media. In Fig. 3, the peak-peak amplitude distribution of all #5 SHA's is plotted vs. the two Born model predictions. The averaging of all 8 SHA amplitudes has evidently stabilized the signal fluctuations resulting from microstructure change. The normal Born model is again shown superior to the weak Born model by predicting closer amplitude to the experiment. The agreement can be made even better, to within 4% error between the experimental average and the normal Born model, by excluding the second SHA amplitude as an outlier.

Table 1. Summary of averaged peak-peak SHA signals and the corresponding standard deviations (denoted by EXPT) of all cases using transducer A. Letter N associated with some cases denotes noise floor in which no SHA signal can be identified, while letter M denotes some SHA signals missed from total 8 SHA's of that size. Values in parentheses and brackets are the corresponding model predictions. ADHC (numbers within []) represents the ad-hoc model and NMBN (numbers within <>) denotes the normal Born model. Measure units are: focal depth - inch, incident angle unit - degree, SHA size - #2=2"/64, #3=3"/64, etc., SHA amplitude - millivolts.

| Focal Depth | Incident Angle | Synthetic Hard-Alpha Inclusion #5 | #4 | #3 | #2 | |
|---|---|---|---|---|---|---|
| 1 | 0 | 624 118 | 393 31 | 246 54M | 177 38N | EXPT |
| | | [542] | [370] | [244] | [80] | ADHC |
| | | <552> | <378> | <209> | <98> | NMBN |
| 1 | 2.5 | 466 86 | 322 26 | 197 24 | 138 28M | |
| | | <403> | <310> | <194> | <91> | |
| 1 | 5 | 201 32 | 169 21 | 150 19 | 91 20 | |
| | | <131> | <146> | <144> | <69> | |
| 1.25 | 0 | 526 95 | 337 26 | 228 43M | 151 24N | |
| | | [484] | [321] | [218] | [67] | |
| | | <512> | <347> | <203> | <82> | |
| 1.25 | 2.5 | 427 65 | 284 23 | 184 23 | 106 17M | |
| | | <388> | <294> | <185> | <78> | |
| 1.25 | 5 | 210 32 | 168 17 | 142 18 | 85 20 | |
| | | <139> | <154> | <146> | <66> | |
| 0.5 | 0 | 494 97 | 292 34 | 181 50M | 155 36N | |
| | | [447] | [300] | [187] | [61] | |
| | | <442> | <293> | <165> | <79> | |
| 0.5 | 2.5 | 353 68 | 244 16 | 137 20 | 112 16M | |
| | | <300> | <234> | <144> | <71> | |
| 0.5 | 5 | 130 23 | 112 17 | 101 12 | 60 9 | |
| | | <93> | <102> | <102> | <50> | |

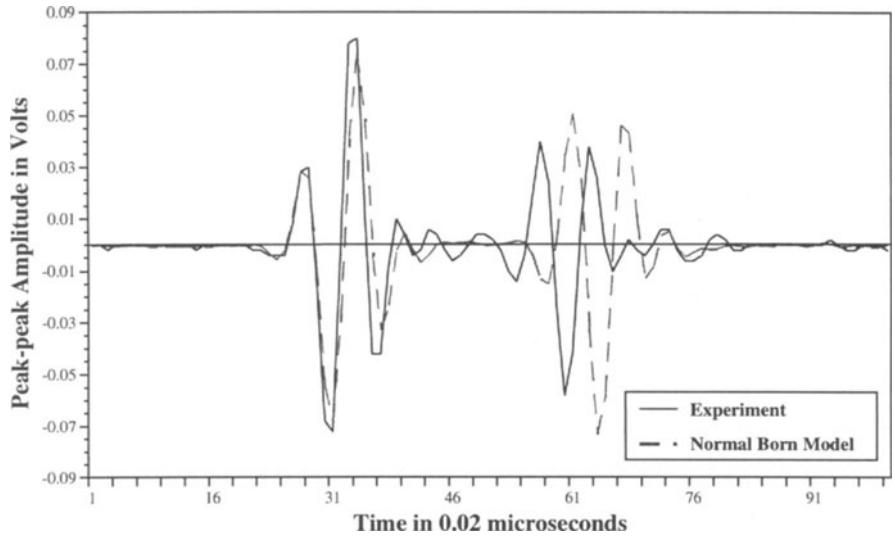


Figure 2. Absolute amplitude and phase comparisons between model and experiment for a typical #5 SHA focused at side-on position using transducer B at normal-incidence.

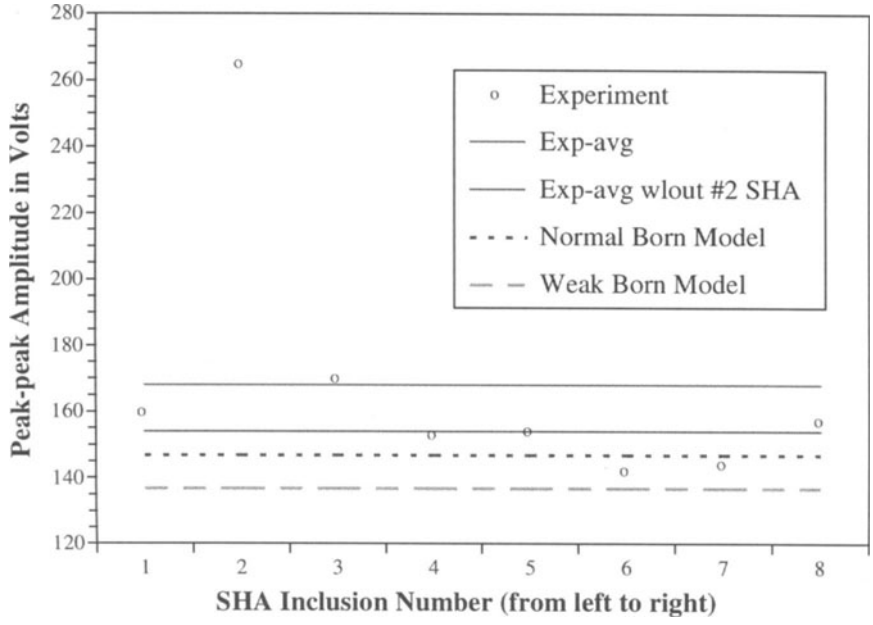


Figure 3. Peak-peak amplitude distribution vs. two Born model predictions for 8 nominal #5 SHA's on focus at 1.625" depth. Transducer B was used at normal incidence.

## MODELING OF "REALISTIC" HARD-ALPHA INCLUSIONS

After the full cycle of ultrasonic model development and laboratory experimental validation was completed, it was natural to proceed with field examination for more realistic testing. As the recent "contaminated billet study" [8] launched, a number of naturally occurring hard-alpha defects are becoming available to test the real strength of the models. Since these natural defect no longer appear in simple, smooth shapes, obtaining the geometrical descriptions of the defects via solid models become fundamentally necessary for the purpose of ultrasonic model calculations. These solid models will be required to provide the complete acoustical and material properties within the volume or on the surface of the defects. In addition to the hard-alpha core, some percentages of these real hard-alpha defects also consist of void, crack and diffusion zones. This further complicates the modeling work as separate solid and ultrasonic models will be needed to deal with these different types of defect components. Much of the information used to construct these solid models will be acquired from the metallographic measurements and chemical analyses which are in turn gained from real defect destructive tests. The most detailed data will come from a set of metallographs of the defect cross section, obtained during an incremental grinding (cut-off) process. Fig. 4 depicts one representative metallographic image showing the various defect components.

As an initial test exercise, we started with two dozens of such metallographic images obtained from the destructive testing of one early hard-alpha field found. These images were taken at even grinding intervals of 5 mils along the defect's axial direction, and have 0.5 mil resolutions on the image planes. For simplicity of this exercise, we consider only the outermost diffusion zone and use its boundary to define the test hard-alpha defect and omit any detailed differences inside. The ultimate objective is certainly to be able to separate these different properties into a classification system. The classification system will be able to determine the number of each kind of feature and where they are located in the block of original titanium material. In this analysis, interpolations of the two-dimensional metallographic image data into a primary three-dimensional surface were performed. Additional extrapolations were then followed to complete the two end portions of the primary surface reconstruction, as in this test exercise no information (images) were available at those portions. The work that has been accomplished so far in the manner is discussed below.

The two-dimensional images were first analyzed to determine the number of regions of interest and their variations from one image to another. For each defect region in an image, a dynamic locator was drawn manually on the computer screen to trace a complete set of discrete boundary points. A linear interpolation was then performed in between the discrete boundary points to normalize the boundary to a fixed N segments. This normalization was carried out by locating a seed position on the boundary at a prescribed orientation. Every successive point on the boundary was set a differential length away from the previous point starting from the seed position. The differential length was equal to the total length of the boundary divided by N-1 points.

After determining the N points on each boundary, a Bezier curve interpolation was performed. The shape of a Bezier curve is defined by an ordered set of data points called control points. The curve approximates the control points but interpolates the first and last control points. A Bezier curve is evaluated by blending the control points with a set of

polynomial blending functions. These properties force the curve to lie completely within the convex hull of the control points. The Bezier blending functions produce a n-th degree polynomial for n+1 control points and force the curve to interpolate through the first and last control points. The curve is tangent to the control point net at the endpoints. The intermediate control points pull the curve in and can be used to modify the shape of the curve. After all Bezier curves are fitted across all defect regions on all images, linear triangular meshes are generated throughout the test hard-alpha body connecting the corresponding boundary points in adjacent images, and the solid model is built. The shaded reconstruction of the test hard-alpha defect is given in Fig. 5.

The ultrasonic model calculation using the geometrical description of this first test solid model is currently underway. Future plans of the solid modeling work will include a number of interpolation algorithms to generate fitted surface of desired smoothness conditions. Extrapolation routines will also be incorporated for completing the defect volume for unknown or missing data. A variety of image processing techniques will be used to automate the determination of the boundary points on the images. A possible intelligent classification system for separating features from one image slice to another will be considered.

ACKNOWLEDGMENTS

The authors would like to thank Drs. Robert Gilmore, Michael Gigliotti and Lee Perocchi of General Electric Corporate Research for providing us with the test transducers, specimen blocks and information of their material and acoustic properties. The authors also thank Dr. Joe Ross of General Electric Aircraft Engine for making the metallographic images available for this research. This material is based upon work performed at Iowa State University as part of the Engine Titanium Consortium operated by Iowa State University, including participants at General Electric, Pratt & Whitney and Allied Signal, and supported by the Federal Aviation Administration Technical Center, Atlantic City, New Jersey, under Grant Number 94G048.

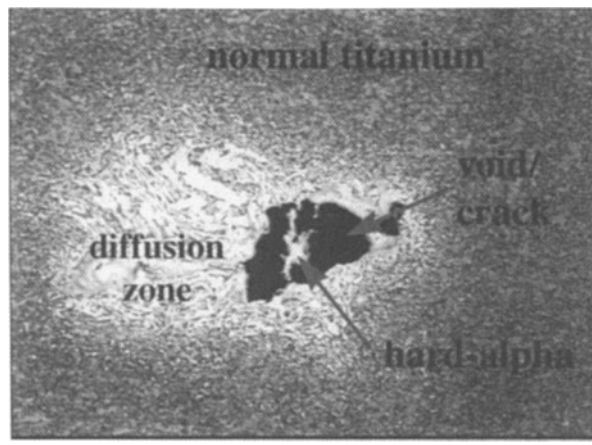


Figure 4. A typical metallographic intensity image of hard-alpha defect.

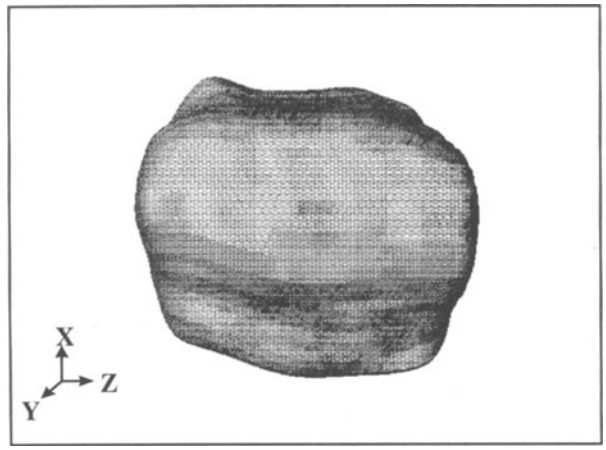


Figure 5. The reconstructed solid model of the test hard-alpha defect. Dimension: 0.3175 (axial Z) by 0.254 (radial X-Y) cm.

## REFERENCES

1. C.-P. Chiou, F. J. Margetan and R. B. Thompson, "Modeling of Ultrasonic Signals from Weak Inclusions," Review of Progress in Quantitative Nondestructive Evaluation, D. O. Thompson and D. E. Chimenti, Eds Vol. 15A, 1996, 49-55.
2. W. Q. Meeker, R. B. Thompson, C.-P. Chiou, S.-L. Jeng and W. T. Tucker, "Methodology for Estimating Nondestructive Evaluation Capability," Review of Progress in Quantitative Nondestructive Evaluation, D. O. Thompson and D. E. Chimenti, Eds Vol. 15B, 1996, 1983-1990.
3. W. Q. Meeker, S.-L. Jeng, C.-P. Chiou and R. B. Thompson, "Improved Methodology for Predicting POD of Detecting Synthetic Hard Alpha Inclusions in Titanium," these volumes.
4. B. A. Auld, "General Electromechanical Reciprocity Relations Applied to the Calculation of Elastic Wave Scattering Coefficients," Wave Motion, 1, 1979, 3-10.
5. R. B. Thompson and T. A. Gray, "A Model Relating Ultrasonic Scattering Measurements Through Liquid-Solid Interfaces to Unbounded Medium Scattering Amplitudes," Journal of Acoustical Society of America, 74 (4), 1983, 1279-1290.
6. B. P. Newberry, R. B. Thompson and E. F. Lopes, "Development and Comparison of Beam Models for Two-Media Ultrasonic Inspection," ," Review of Progress in Quantitative Nondestructive Evaluation, D. O. Thompson and D. E. Chimenti, Eds Vol. 6A, 1987, 639-647.
7. C.-P. Chiou, F. J. Margetan and R. B. Thompson, "Ultrasonic Signal Characterizations of Flat-bottom Holes in Titanium Alloys: Experiment and Theory," Review of Progress in Quantitative Nondestructive Evaluation, D. O. Thompson and D. E. Chimenti, Eds Vol. 14B, 1995, 2121-2128.
8. L. Brasche, K. Smith and J. Bartos, "An Overview of the Contaminated Billet Study," these volumes.